Wünsch, J., Thomas, M., Gruber, T. (2001): Simulation of oceanic bottom pressure for gravity space missions. - Geophysical Journal International, 147, 2, pp. 428—434.

DOI: http://doi.org/10.1046/j.1365-246X.2001.00551.x

Geophys. J. Int. (2001) **147,** 428–434

Simulation of oceanic bottom pressure for gravity space missions

J. Wünsch,[1] M. Thomas[2] and Th. Gruber[1]

[1] *GeoForschungsZentrum Potsdam, Division Kinematics and Dynamics of the Earth, Telegrafenberg,* D-14473 *Potsdam, Germany. E-mail: wuen@gfz-potsdam.de*

[2] *Institut für Meereskunde, Universität Hamburg, Troplowitzstrasse* 7, D-22529 *Hamburg, Germany*

Accepted 2001 June 27. Received 2001 June 27; in original form 2000 February 26

SUMMARY

Oceanic bottom pressure is affected by mass redistribution in the ocean and atmosphere, and it influences gravity field determinations by the new satellite missions CHAMP, GRACE and GOCE from seasonal up to short-period timescales. Thus, mass redistribution in the ocean needs to be accounted for to obtain the mean gravity field.

With the Hamburg ocean model for circulation and tides (OMCT), time-dependent oceanic bottom pressure fields are calculated using atmospheric fluxes of momentum, heat and freshwater from ECHAM3 real-time simulations. The resulting bottom pressure fields are expanded in gravity field spherical harmonic coefficients as a function of time. The temporal resolution is 5 days for extracting annual and semi-annual amplitudes and 6 hr for studying high-frequency variations.

In order to estimate the influence of oceanic mass variations on gravity field determination, degree variance spectra of simulated bottom pressure are calculated and compared with the expected error spectra of space missions. Furthermore, variations in geoid height ΔN from the modelled Stokes coefficients are illustrated. The numerical results suggest that ocean-induced long-wavelength gravity variations become detectable with the CHAMP and GRACE gravity missions.

Key words: ocean circulation, Stokes coefficients, time-variable gravity field.

1 INTRODUCTION

The Earth's gravity field varies in time due to mass redistributions within and mass exchange between the subsystems. Apart from dynamic processes within the solid Earth, the main sources of these variations are time-dependent surface air pressure and oceanic bottom pressure, soil moisture, snow load, groundwater and ice. Here we concentrate on the role of the time-variable oceanic bottom pressure, which acts like a surface mass load for the external gravity field.

There has been some previous work in this area. Wahr *et al.* (1998) considered the time-variable gravity field of the Earth caused by the redistribution of mass by means of hydrological, oceanographic and atmospheric models. For the ocean they used a variant of the POP (Parallel Ocean Program) model developed at Los Alamos National Laboratory. Wahr *et al.* (1998) calculated annual geoid amplitudes of cos ωt and sin ωt on the global scale ($\omega = 2\pi/1.00\text{yr}$).

Ponte (1999) derived the seasonal cycle in bottom pressure, p_b, over the global ocean from the POCM_4B (Parallel Ocean Climate Model) simulation (Semtner & Chervin 1992; Stammer *et al.* 1996). The estimated seasonal large-scale p_b signals had amplitudes ranging from less than 1 cm of water over most of the deep ocean to several centimetres over shelves. Variability generally increased towards the western sides of the basins and was also larger in some Southern Ocean regions. An oscillation between subtropical and higher latitudes in the North Pacific turned out to be significant.

Johnson (1998) and Johnson *et al.* (2001) studied non-tidal oceanic contributions to gravity field changes as predicted by the POCM_4B model. As in the papers mentioned above, Johnson *et al.* (2001) employed a so-called Greatbatch correction: the ocean model is formulated using the Boussinesq approximation and consequently conserves oceanic volume rather than mass. As Greatbatch (1994) suggested, sea surface height is adjusted at each time step by adding a global layer of uniform thickness in order to correct for this. The thickness of the additional layer is determined by requiring that the total oceanic mass is constant. Following Johnson (1999, private communication), for annual and semi-annual signals this correction affects only the coefficients $\bar{C}_{10}$ and $\bar{C}_{20}$ appreciably. (Of course, $\bar{C}_{00}$ becomes exactly zero after the correction has been applied.)

Gruber *et al.* (2000) used ERS-1 altimetry corrected for the thermal expansion of water as well as the POCM model to estimate fully normalized Stokes coefficients $\bar{C}_{nm}$, $\bar{S}_{nm}$ (e.g. Torge 1980; Heiskanen & Moritz 1967) plus degree variance spectra due to oceanic mass redistribution. These simulations indicated the order of magnitude of geoid height variations to be anticipated for CHAMP and GRACE. The Stokes coefficients $\bar{C}_{nm}$, $\bar{S}_{nm}$ are defined in the expansion of the gravitational

potential V outside the Earth in spherical coordinates r, λ, φ as

$$V(r, \lambda, \varphi) = \frac{GM}{r}\left[1 + \sum_{n=1}^{\infty}\sum_{m=0}^{n}\left(\frac{a}{r}\right)^n (\bar{C}_{nm}\cos m\lambda + \bar{S}_{nm}\sin m\lambda) P_{nm}(\sin\varphi)\right], \quad (1)$$

where a is the equatorial radius of the Earth, G is the constant of gravitation, M is the mass of the Earth and P_{nm} are the fully normalized Legendre functions.

Cazenave *et al.* (1999) considered space geodesy-derived annual variations of the long-wavelength geoid. They compared this to hydrometeorological loading data (atmospheric surface pressure, snow and soil moisture load, and ocean mass load). For ocean mass load, TOPEX/POSEIDON altimetry was employed together with a steric correction.

With the hydrostatic equation the oceanic bottom pressure, p_b, at a point with geographic longitude λ and latitude φ can be written as

$$p_b = g\int_{-H}^{\zeta} \rho\, dz + p_a \approx g\rho_0\zeta + g\int_{-H}^{0} \rho\, dz + p_a\,, \quad (2)$$

where g is the acceleration due to gravity, H is the depth of water, ζ is the water elevation at the surface, ρ is the density of the sea water, ρ_0 is the mean density of sea water and p_a is the atmospheric surface pressure.

In this paper we investigate seasonal, subseasonal and high-frequency variations of the modelled ocean bottom pressure fields and their impact on the global gravity field in terms of Stokes coefficients and geoid height variations. Special emphasis is given to annual, semi-annual and third-annual geoid variations as well as to randomly selected differences of consecutive days. Here, it is assumed that the ocean's response to atmospheric surface pressure is exactly that of an inverted barometer. This means that in eq. (2) the atmospheric pressure component is set to 0 ($p_a = 0$) (Lambeck 1988, p.114; Wunsch & Stammer 1997). The extent to which the inverted barometer approximation holds has been discussed by Fu & Pihos (1994), Gaspar & Ponte (1997) and more recently by Ponte & Gaspar (1999). The authors are in agreement that the sea level response is generally somewhat weaker than Inverted Barometer (IB) at high frequencies. Significant deviations from the IB assumption were identified, particularly in some regions of the Southern Ocean and in the tropics, were the regression coefficient dropped to about -0.75 cm mbar^{-1}. They concluded that most of the apparent non-IB response in the extratropics was caused by the effects of wind forcing, which is strongly correlated with pressure. However, atmospheric pressure variability is extremely small in the tropics (rms ≤ 2 mbar), thus the error arising from the IB approximation, i.e. $p_a = 0$, is also very small in this region.

2 SPACE MISSIONS FOR GRAVITY

The currently operating and upcoming gravity field missions CHAMP, GRACE and GOCE are sensitive to short- and long-term gravity variations from various sources in, on and above the Earth. Depending on the mission profiles, each of the three missions is differently sensitive to these signals. The first of these missions, CHAMP, which was successfully launched into a near-polar orbit on July 15 2000 (Reigber *et al.* 2000) carries, besides other instruments for magnetic field monitoring, a GPS receiver and an accelerometer for gravity field determination. The continuous GPS tracking of the satellite together with measurements of the non-gravitational forces by the accelerometer enables a gravity field improvement of one order of magnitude in accuracy for the long wavelengths with respect to current knowledge. Considering a planned mission lifetime of 5 yr it is expected that very long-wavelength gravity variations will be detectable with CHAMP.

The dual-satellite GRACE mission (Tapley & Reigber 2000), scheduled for launch at the end of 2001, will provide, in addition to the GPS and accelerometer measurements, high-precision microwave range measurements (micrometre accuracy) and their variations between the two satellites. Simulation studies show that a further gravity field improvement of 1–2 orders of magnitude and an increase of spatial resolution with respect to the CHAMP sensitivity can be expected. For estimating variations in the gravity field, it is planned to compute monthly solutions for the planned lifetime of 5 yr. By analysing the series of monthly models, new insight into the global water cycle should be provided. In 2005 the ESA gradiometry mission GOCE (ESA 1999; Rummel *et al.* 2000) is planned for launch. This mission will directly measure the gravity tensor in space, which can then be used to estimate the high-resolution static Earth gravity field. For the GOCE mission two measurement periods of 6 months each, separated by a 5 month interruption are foreseen. Short- and long-term gravity variations have to be removed prior to the final gravity field computation from the gradiometer data in order to determine the real static field.

All three missions are strongly related to signals coming from variations in the gravity field. As mentioned above, the CHAMP and GRACE missions will provide time-series of monthly or longer gravity field solutions. The changes in these solutions represent the integrated effect of all mass variations in, on and above the Earth. If the integrated effect can be separated into its major sources, these can be used, for example, to validate and improve oceanic, hydrological and ice mass models. On the other hand, all three missions rely strongly on atmospheric and oceanic models for the removal of short-term gravity variations with timescales below one month, which would map into the gravity field solutions because of the time–space sampling. Consequently, the quality of atmospheric and oceanic models has a direct impact on the final gravity field model quality. This clearly shows the strong relation between gravity field determination with the new space missions and ocean modelling. As one of the optional ocean models to be used for de-aliasing short-term gravity variations, the Hamburg OMCT may be used, which is further described in the next section.

3 THE OCEAN CIRCULATION MODEL, OMCT

The ocean model used here is the Hamburg Ocean Model for Circulation and Tides (Thomas & Sündermann 1998, 2000; Thomas *et al.* 2001), which was developed by coupling an extended version of the climatological model of Drijfhout *et al.* (1996) with an ephemeral tidal model. It is based on the non-linear balance equations for momentum, the equation of continuity for an incompressible fluid and conservation equations for heat and salt. The hydrostatic as well as the Boussinesq approximation are employed. Prognostic variables are sea

surface elevation, horizontal velocities, temperature, salinity, and sea ice thickness and compactness (Hibler, 1979). The resolution of the numerical grid is 1.875° in longitude and latitude, 13 layers exist in the vertical and the time step used here is 1 hr. For the present work a model run with circulation only (without ocean tides) was used.

Initially, the OMCT was spun up for about 260 yr with cyclic boundary conditions, that is, climatological wind stresses (Hellerman & Rosenstein 1983) as well as annual mean surface temperatures and salinities (Levitus 1982). Starting from this steady-state circulation, twice-daily atmospheric real-time forcing fields from ECHAM3 simulations (Roeckner *et al.* 1992) were applied that consist of wind stress components, surface temperatures and freshwater fluxes. These forcing fields are the result of a long time simulation from 1949 to 1994 of the ECHAM3-T21 atmospheric general circulation model (Roeckner *et al.* 1992), which was driven by monthly means of observed sea surface temperatures and global ice coverage from the GISST2.2 data set (Parker *et al.* 1994) of the Hadley Centre for Climate Prediction and Research in Bracknell. In order to avoid an unrealistic mass drift, salinity was restored to the annual mean sea surface salinity according to Levitus (1982) using a timescale of 38 days.

We did not yet employ a Greatbatch (1994) correction (see the Introduction) to the OMCT runs. As mentioned above, in this investigation forcing by atmospheric surface pressure was not accounted for. Wünsch (2000) computed the oceanic contribution to the annual (period = 1.00 yr) polar motion of the Earth using an OMCT run that included atmospheric pressure forcing. In the meantime these polar motion calculations have been repeated under the assumption $p_a = 0$.

4 SPHERICAL HARMONIC ANALYSIS AND RESULTS

Oceanic bottom pressure acts as a surface mass load $q = p_b/g$ with units of kg m^{-2}; $g = 9.806$ m s^{-2} is the acceleration due to gravity. According to Gegout & Cazenave (1993) and Dong *et al.* (1996), the Stokes coefficients can be obtained as a surface integral over the sphere:

$$\delta\bar{C}_{nm} = \frac{1+k'_n}{2n+1}\,\frac{a^2}{M}\int q(\lambda,\varphi)\cos(m\lambda)P_{nm}(\sin\varphi)\,dS\,, \qquad (3)$$

where a is the equatorial Earth radius, M is the mass of the Earth, n is the Legendre degree, k'_n is the loading Love number of degree n and P_{nm} are the normalized Legendre functions. A similar equation holds for $\delta\bar{S}_{nm}$, where sin $(m\lambda)$ occurs instead of cos $(m\lambda)$.

By numerical integration of bottom pressure block mean values over the sphere in the sense of eq. (3), the coefficients $\delta\bar{C}_{nm}$, $\delta\bar{S}_{nm}$ were calculated during the OMCT simulations. Over continents we set $p_b = 0$. Numerical values for the loading Love numbers k'_n were taken from Dong *et al.* (1996) for $n = 2$–9 and from Farrell (1972) for $n = 10$–50. Fully normalized spherical harmonic functions Y_{nm} according to Heiskanen & Moritz (1967) were used.

4.1 Seasonal gravity variations

For some of the lowest-order Stokes coefficients a trigonometric fit was calculated from two model years (1978 and 1979) by the method of least squares to obtain annual and semi-annual amplitudes. The formulation also contained a constant plus a linear trend that occurs because of modelling reasons. All *a priori* weights were chosen equal. Two years of model data is a good choice to extract the annual and semi-annual waves from each small time-series of $\bar{C}_{nm}(t)$ or $\bar{S}_{nm}(t)$. The results are given in Table 1 for real-time forcing and in Table 2 for climatological forcing. Typical orders of magnitude for real-time forcing are 3×10^{-11} in the annual amplitude and 1.5×10^{-11} in the semi-annual amplitude. The amplitudes of the climatological result are clearly smaller than those with real-time forcing. This is to be expected, since as a consequence of long-time averaging, climatological forcing fields tend to be smoother than real-time forcing fields and thus cannot show as much variation. [Some polar motion work uses 'climatological' $\bar{C}_{21}(t)$, $\bar{S}_{21}(t)$ to study the excitation of the Chandler wobble.] The phase angles φ have no clear relation between the results for climatological and real-time forcing. Error estimates for amplitude A are $\pm0.17\times10^{-11}$ (Table 1) and $\pm0.10\times10^{-11}$ (Table 2), both annual and semi-annual. Thus, most entries in these tables are significant.

Fig. 1 shows as an example $\delta\bar{C}_{50}(t)$ for two model years with real-time forcing and the corresponding curve for climatological forcing. Annual and semi-annual components are visible plus a small linear numerical trend. As a preparation and comparison for the next section, we give in Fig. 2 degree variance spectra obtained by forming differences for time intervals of 1 wk, 1 month, 0.5 yr and 1 yr. Fig. 2 comprises the annual and semi-annual periods, which are shown in detail in Table 1.

Table 1. Fully normalized Stokes coefficients $\bar{C}_{nm}$, $\bar{S}_{nm}$ caused by oceanic bottom pressure (data from the OMCT model; real-time forcing); annual plus semi-annual trigonometric fit from two model years (1978 and 1979). Amplitudes A are $\times10^{-11}$ and phase angle φ is in degrees. Convention for φ: $A\cos(\omega t-\varphi)$. The estimated standard deviation of A is $\pm0.17\times10^{-11}$ for both annual and semi-annual.

Coeff.	Annual		Semi-annual	
	A	φ	A	φ
C_{00}	3.90	56	1.64	26
C_{10}	6.01	256	3.11	296
C_{11}	5.32	353	2.60	212
C_{20}	4.54	6	0.41	121
C_{21}	3.72	223	1.41	152
C_{22}	0.53	38	0.69	317
C_{30}	0.84	84	0.28	37
C_{31}	0.23	159	0.40	4
C_{32}	2.26	224	0.46	139
C_{33}	0.80	309	0.31	265
C_{40}	1.33	26	1.40	37
C_{50}	3.02	25	0.10	152
C_{52}	0.42	304	0.47	49
C_{55}	0.36	163	0.17	97
C_{60}	0.36	232	0.33	223
S_{11}	4.24	250	1.68	110
S_{21}	1.80	226	0.82	212
S_{22}	3.68	216	0.50	221
S_{31}	0.33	118	0.13	166
S_{32}	1.68	261	0.59	187
S_{33}	1.52	224	0.52	198
S_{52}	0.30	107	0.18	39
S_{55}	0.49	250	0.18	179

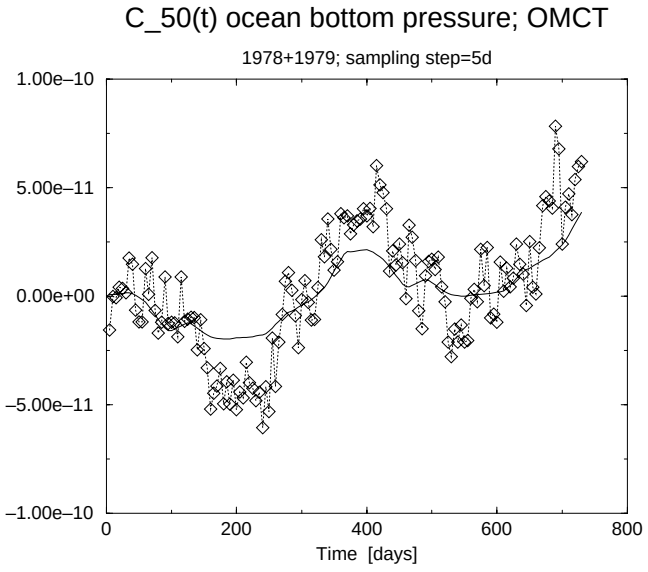

Figure 1. The oceanic Stokes coefficient $\delta\bar{C}_{50}$ as a function of time over two model years. Dotted curve with diamonds: real-time forcing; continuous curve: climatological forcing. A constant has been subtracted from both curves.

Table 2. Fully normalized Stokes coefficients $\bar{C}_{nm}$, $\bar{S}_{nm}$ caused by oceanic bottom pressure (data from the OMCT model; climatological forcing); annual plus semi-annual trigonometric fit. Amplitudes A are $\times 10^{-11}$ and phase angle φ is in degrees. Convention for φ: $A\cos(\omega t-\varphi)$. The estimated standard deviation of A is $\pm 0.10\times 10^{-11}$ for both annual and semi-annual.

Coeff.	Annual		Semi-annual	
	A	φ	A	φ
C_{00}	10.53	277	1.20	127
C_{10}	1.59	78	1.93	2
C_{11}	1.27	90	0.73	251
C_{20}	2.07	346	1.23	341
C_{21}	2.17	222	0.29	353
C_{22}	2.19	30	0.14	19
C_{30}	1.50	185	1.13	86
C_{33}	1.41	351	0.034	332
C_{40}	1.34	139	0.85	2
C_{50}	1.40	22	0.30	28
C_{52}	0.04	13	0.33	342
C_{55}	0.71	186	0.13	44
C_{60}	0.21	9	0.15	63
S_{11}	1.83	213	0.61	260
S_{21}	0.96	308	0.13	245
S_{22}	2.34	215	0.20	236
S_{33}	0.31	332	0.31	7
S_{52}	0.20	69	0.25	314
S_{55}	0.18	326	0.12	313

4.2 High-frequency variations

In order to study high-frequency temporal variations in the Stokes coefficients and the resulting geoid, daily differences of coefficients for randomly selected days over one model year of output (1994) were determined. For these coefficient differences a degree variance spectrum was computed and compared to the predicted error spectrum for the CHAMP and GRACE missions. According to Fig. 3, the signal of daily gravity variations is above the error spectrum up to degree 8 for CHAMP and up to degree 34 for GRACE. Thus, the ocean shows not only seasonal but also strong high-frequency gravity signals. This high-frequency variability means that these gravity variations have to be removed during the gravity field inversion from the measured signal in order to derive a monthly or multiyear mean gravity field model (Hughes *et al.* 2000). To visualize and analyse the daily gravity variations, Stokes coefficients were

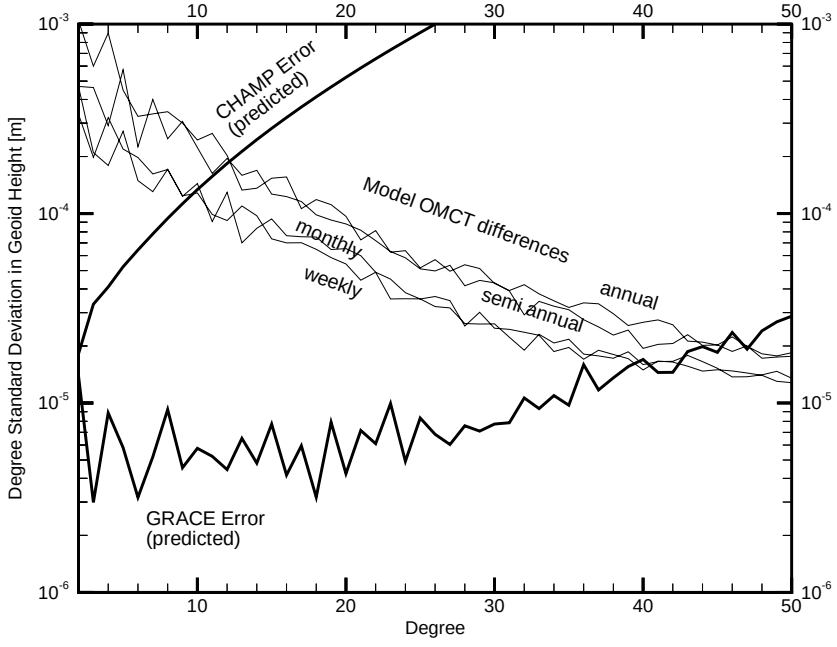

Figure 2. Degree variance spectrum of oceanic weekly, monthly, semi-annual and annual differences expressed as geoid height (model year 1994).

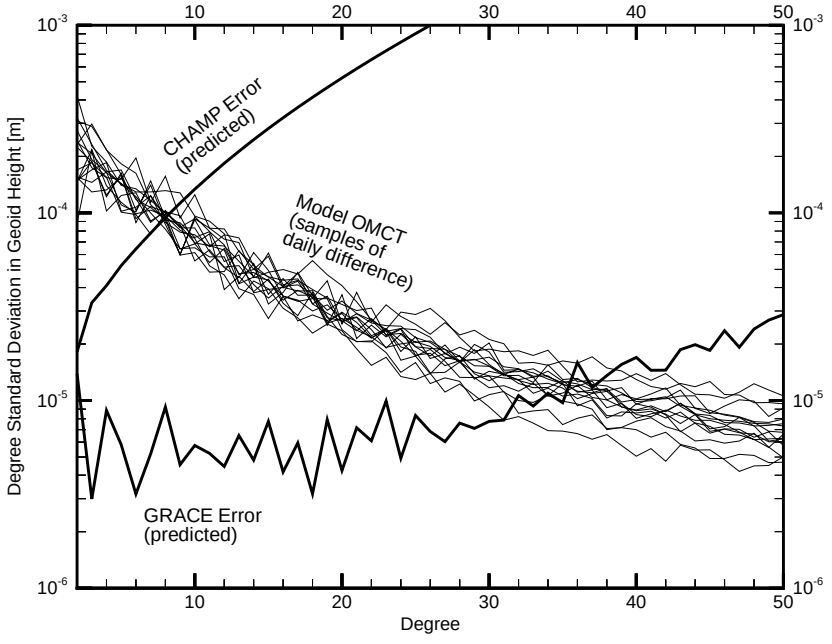

Figure 3. Degree variance spectrum of oceanic daily differences expressed as geoid height (model year 1994).

converted to geoid heights using the formula

$$\Delta N(\lambda, \varphi) = a \sum_{n=2}^{50} \sum_{m=0}^{n} (\delta \bar{C}_{nm} \cos m\lambda + \delta \bar{S}_{nm} \sin m\lambda) P_{nm}(\sin \varphi) \tag{4}$$

(Torge 1980). Thus, for each 6 hourly coefficient set over the full year 1994, geoid heights with respect to a mean geoid were computed, illustrated and finally merged in an animation. This animation clearly shows the annual cycle and superimposed high-frequency variations. The geoid height typically varies in the range -5 to $+5$ mm. In contrast to the seasonal signal, circulation-induced short-period anomalies are—with the exception of the diurnal cycle—not forced by a defined frequency and, therefore, cannot be related definitively to a periodic physical process responsible for the anomaly. The snapshots of Fig. 4 demonstrate the time-dependent development of simulated geoid heights over 3 weeks. Apart from disturbances in the Mediterranean and Bering seas, which cannot be accounted for as a consequence of the coarse horizontal resolution, amplitudes of geoid height anomalies are most pronounced near western boundary currents and in the sphere of influence of the Antarctic Circumpolar Current. The latter coincidence may be interpreted as a relation between geoid height anomalies and variations of the wind-driven circulation, since changes of wind stress components cause variations of the geostrophic sea level as well as instabilities of the velocity field. However, the assumed correlation has still to be confirmed quantitatively.

5 CONCLUSIONS

Based on ocean bottom pressure fields as output of the Hamburg OMCT baroclinic ocean model, time-series of Stokes coefficients for different time and spatial resolutions were computed. From analyses performed with these time-series the following conclusions can be made.

(i) The annual and semi-annual amplitudes of the low-order Stokes coefficients are of the order of 3×10^{-11} (annual) and 1.5×10^{-11} (semi-annual) for real-time forcing.

(ii) When using climatological forcing, these amplitudes are 1.5×10^{-11} (annual) and 1×10^{-11} (semi-annual).

(iii) A degree variance spectrum of the daily differences shows a pronounced high-frequency variability in the oceanic contribution to gravity changes. This is detectable with CHAMP and with the missions in preparation (GRACE and GOCE) in different frequency ranges. For all missions these short-term variations have to be removed prior to the final analysis to make sure that a mean field over a desired time period (e.g. 1 month) is determined. To run the OMCT model for this purpose in an operational framework is one of the options that are currently being investigated.

(iv) The corresponding oceanic geoid height changes are in the interval -5 to $+5$ mm as demonstrated by maps of geoid height. It becomes obvious that even in quiet regions (from an oceanographic point of view), small geoid variations that are caused by mass variations in more distant zones are present. Generally, the well-known oceanographic features such as western boundary currents as well as the Antarctic Circumpolar Current are visible.

When CHAMP and GRACE data become available, the problem of ocean-induced gravity field variations has to be considered further. The data and model outputs have to be validated against each other in order to reach a common accuracy level in all processing steps.

ACKNOWLEDGMENTS

We thank Dr H. Greiner-Mai, Prof. H. Jochmann and Dr P. Schwintzer (all at GFZ Potsdam) for useful discussions. JW is supported by DFG grant RE 536/7-2 and MT acknowledges DFG grant Br 675/8-2. We thank the Meteorological

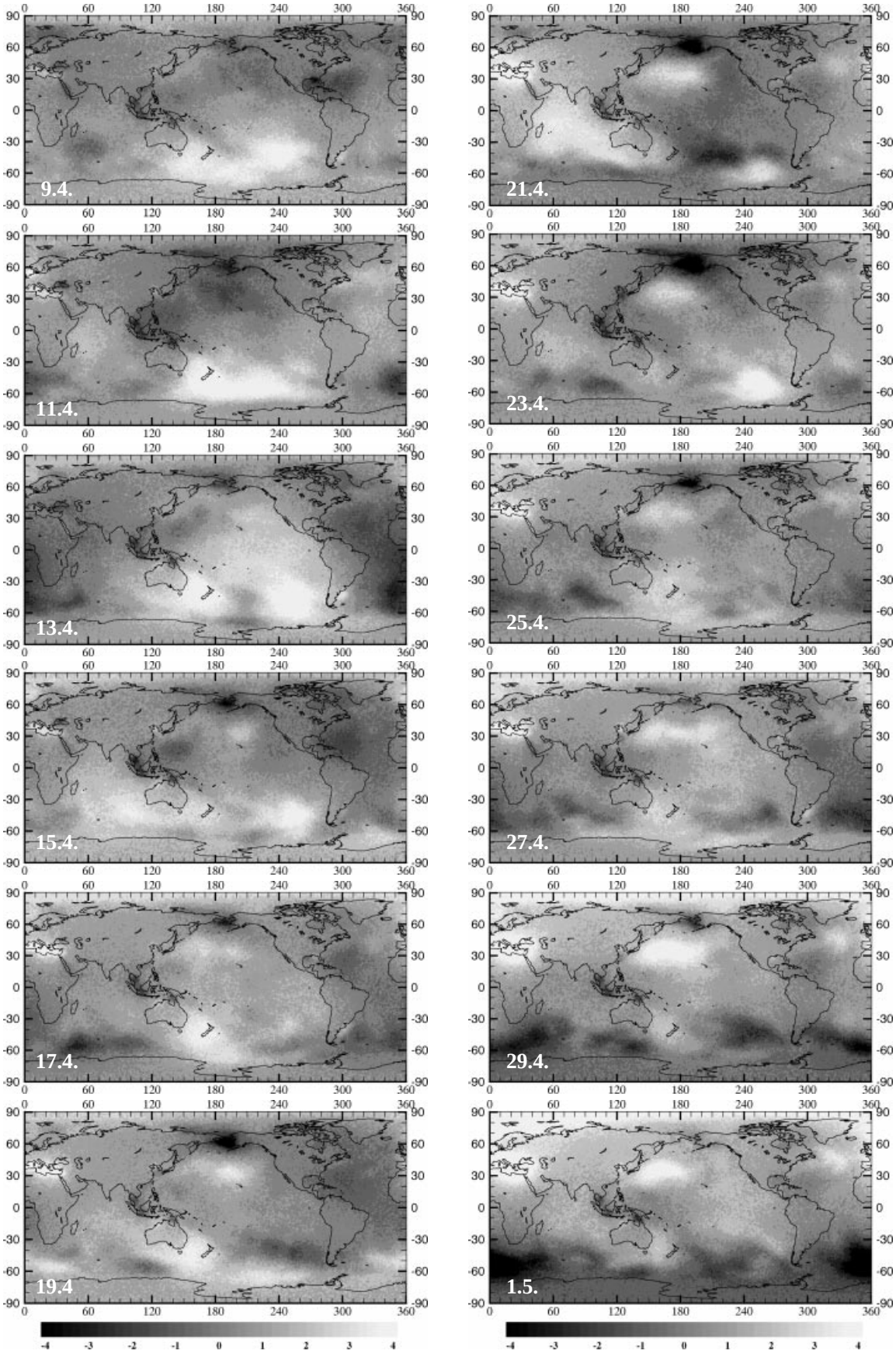

Figure 4. Geoid height maps at 2 day intervals for a selected period in 1994 caused by oceanic mass redistribution derived from the OMCT model (mm).

Institute of the University of Bonn, Germany, and the Deutsche Klimarechenzentrum, Hamburg, Germany, for providing data from the ECHAM3-T21 simulations.

REFERENCES

Cazenave, A., Mercier, F., Bouille, F. & Lemoine, J.M., 1999. Global-scale interactions between the solid Earth and its fluid envelopes at the seasonal time scale, *Earth planet. Sci. Lett.,* **171,** 549–559.

Dong, D., Gross, R.S. & Dickey, J.O., 1996. Seasonal variations of the Earth's gravitational field: an analysis of atmospheric pressure, ocean tidal, and surface water excitation, *Geophys. Res. Lett.,* **23,** 725–728.

Drijfhout, S., Heinze, C., Latif, M. & Maier-Reimer, E., 1996. Mean circulation and internal variability in an ocean primitive equation model, *J. Phys. Oceanogr.,* **26,** 559–580.

ESA, 1999. The four candidate earth explorer core missions—gravity field and steady state ocean circulation, *ESA SP-1233(1)*.

Farrell, W.E., 1972. Deformation of the earth by surface loads, *Rev. Geophys. Space Phys.,* **10,** 761–797.

Fu, L.-L. & Pihos, G., 1994. Determining the response of sea level to atmospheric pressure forcing using TOPEX/POSEIDON data, *J. geophys. Res.,* **99** (C12), 24 633–24 642.

Gaspar, P. & Ponte, R.M., 1997. Relation between sea level and barometric pressure determined from altimeter data and model simulations, *J. geophys. Res.,* **102** (C1), 961–971.

Gegout, P. & Cazenave, A., 1993. Temporal variations of the Earth's gravity field for 1985-1989 derived from LAGEOS, *Geophys. J. Int.,* **114,** 347–359.

Greatbatch, R.J., 1994. A note on the representation of steric sea level in models that conserve volume rather than mass, *J. geophys. Res.,* **99** (C6), 12 767–12 771.

Gruber, Th., Reigber, Ch. & Wünsch, J., 2000. Estimation of ocean mass redistribution by means of altimetry and circulation models and its impact on the gravity field, in *Towards an Integrated Global Geodetic Observing System (IGGOS),* pp. 218–221, eds Rummel, R., Drewes, H., Bosch, W. & Hornik, H., *IAG Symp. 120,* Springer-Verlag, Berlin.

Heiskanen, W.A. & Moritz, H., 1967. *Physical Geodesy,* W. H. Freeman, San Francisco, CA.

Hellerman, S. & Rosenstein, M., 1983. Normal monthly wind stress over the world ocean with error estimates, *J. Phys. Oceanogr.,* **13,** 1093–1104.

Hibler, W.D., 1979. A dynamic thermodynamic sea ice model, *J. Phys. Oceanogr.,* **9,** 815–846.

Hughes, C.W., Wunsch, C. & Zlotnicki, V., 2000. Satellite peers through the oceans from space, *EOS, Trans. Am. geophys. Un.,* **81,** 68.

Johnson, T.J., 1998. The role of the ocean in the planetary angular momentum budget, *PhD thesis,* University of Texas, Austin, TX.

Johnson, T.J., Wilson, C.R. & Chao, B.F., 2001. Non-tidal oceanic contributions to gravity field changes: predictions of the POCM, *J. geophys. Res.,* **106** (B6), 11 315–11 334.

Lambeck, K., 1988. *Geophysical Geodesy,* Oxford University Press, Oxford.

Levitus, S., 1982. *Climatological Atlas of the World Ocean, NOAA Prof. Pap.* 13*,* US Department of Commerce, Washington DC.

Parker, D.E., Jones, P.D., Folland, C.K. & Bevan, A., 1994. Interdecadal changes of surface temperature since the late nineteenth century, *J. geophys. Res.,* **99** (D7), 14 373–14 399.

Ponte, R.M., 1999. A preliminary model study of the large-scale seasonal cycle in bottom pressure over the global ocean, *J. geophys. Res.,* **104** (C1), 1289–1300.

Ponte, R.M. & Gaspar, P., 1999. Regional analysis of the inverted barometer effect over the global ocean using TOPEX/POSEIDON data and model results, *J. geophys. Res.,* **104** (C7), 15 587–15 602.

Reigber, Ch., Lühr, H. & Schwintzer, P., 2000. Status of the CHAMP mission, in *Towards an Integrated Global Geodetic Observing System (IGGOS),* pp. 63–65, eds Rummel, R., Drewes, H., Bosch, W. & Hornik, H., *IAG Symp. 120,* Springer-Verlag, Berlin.

Roeckner, E., *et al.*, 1992. Simulation of the present-day climate with the ECHAM model: impact of the model physics and resolution, *Report,* No. 93*,* Max-Planck-Institut für Meteorologie, Hamburg.

Rummel, R., Müller, J., Oberndorfer, H. & Sneeuw, N., 2000. Satellite gravity gradiometry with GOCE, in *Towards an Integrated Global Geodetic Observing System (IGGOS),* pp. 66–72, eds Rummel, R., Drewes, H., Bosch, W. & Hornik, H., *IAG Symp. 120,* Springer-Verlag, Berlin.

Semtner, A.J. & Chervin, R.M., 1992. Ocean circulation from a global eddy-resolving model, *J. geophys. Res.,* **97** (C4), 5493–5550.

Stammer, D., Tokmakian, R., Semtner, A. & Wunsch, C., 1996. How well does a 1/4 degree global circulation model simulate large-scale oceanic observations?, *J. geophys. Res.,* **101** (C10), 25 779–25 811.

Tapley, B.D. & Reigber, Ch., 2000. The GRACE Mission: status and future plans, *EOS, Trans. Am. geophys. Un.,* **81,** F307 (suppl.).

Thomas, M. & Sündermann, J., 1998. Zur simultanen Modellierung von allgemeiner Zirkulation und Gezeiten im Ozean und Auswirkungen auf bestimmte Erdrotationsparameter, in *Progress in Geodetic Science,* pp. 144–151, ed. Freeden, W., Shaker Verlag, Aachen.

Thomas, M. & Sündermann, J., 2000. Numerical simulations of ocean induced variations of Earth's rotation, in *Proc. Journées 1999 & IX. Lohrmann-Kolloquium,* pp. 167–169, eds Soffel, M. & Capitaine, N., Observatoire de Paris, Paris.

Thomas, M., Sündermann, J. & Maier-Reimer, E., 2001. Consideration of ocean tides in an OGCM and impacts on subseasonal to decadal polar motion excitation, *Geophys. Res. Lett.,* **28,** 2457–2460.

Torge, W., 1980. *Geodesy,* de Gruyter, Berlin.

Wahr, J.M., Molenaar, M. & Bryan, F., 1998. Time variability of the Earth's gravity field: hydrological and oceanic effects and their possible detection using GRACE, *J. geophys. Res.,* **103** (B12), 30 205–30 229.

Wunsch, C. & Stammer, D., 1997. Atmospheric loading and the oceanic 'inverted barometer' effect, *Rev. Geophys.,* **35,** 97–107.

Wünsch, J., 2000. Oceanic influence on the annual polar motion, *J. Geodyn.,* **30,** 389–399.